# Digital signal processor-based high-precision on-line Voigt lineshape fitting for direct absorption spectroscopy

AIP | Review of Scientific Instruments

# Digital signal processor-based high-precision on-line Voigt lineshape fitting for direct absorption spectroscopy

Lijun Xu, Chang Liu, Deyan Zheng, Zhang Cao, and Weiwei Cai

Citation: Review of Scientific Instruments **85**, 123108 (2014); doi: 10.1063/1.4903356
View online: http://dx.doi.org/10.1063/1.4903356
View Table of Contents: http://scitation.aip.org/content/aip/journal/rsi/85/12?ver=pdfcov
Published by the AIP Publishing



# Digital signal processor-based high-precision on-line Voigt lineshape fitting for direct absorption spectroscopy

Lijun Xu,[1,a)] Chang Liu,[1] Deyan Zheng,[1] Zhang Cao,[1] and Weiwei Cai[2]
[1]*Ministry of Education's Key Laboratory of Precision Opto-mechatronics Technology, School of Instrumentation and Opto-Electronic Engineering, Beihang University, Beijing 100191, China*
[2]*Department of Chemical Engineering and Biotechnology, University of Cambridge, Cambridge CB2 3RA, United Kingdom*

(Received 29 September 2014; accepted 24 November 2014; published online 10 December 2014)

To realize on-line high-accuracy measurement in direct absorption spectroscopy (DAS), a system-on-chip, high-precision digital signal processor-based on-line Voigt lineshape fitting implementation is introduced in this paper. Given that the Voigt lineshape is determined by the Gauss full width at half maximum (FWHM) and Lorentz FWHM, a look-up table, which covers a range of combinations of both, is first built to achieve rapid and accurate calculation of Voigt lineshape. With the look-up table and raw absorbance data in hand, Gauss-Newton nonlinear fitting module is implemented to obtain the parameters including both the Gauss and Lorentz FWHMs, which can be used to calculate the integrated absorbance. To realize the proposed method in hardware, a digital signal processor (DSP) is adopted to fit the Voigt lineshape in a real-time DAS measurement system. In experiment, temperature and $H_2O$ concentration of a flat flame are recovered from the transitions of 7444.36 $cm^{-1}$ and 7185.6 $cm^{-1}$ by the DSP-based on-line Voigt lineshape fitting and on-line integral of the raw absorbance, respectively. The results show that the proposed method can not only fit the Voigt lineshape on-line but also improve the measurement accuracy compared with those obtained from the direct integral of the raw absorbance. © *2014 AIP Publishing LLC*. [http://dx.doi.org/10.1063/1.4903356]

## I. INTRODUCTION

As a fast, sensitive, non-intrusive, and cost-effective optical sensing technique, direct absorption spectroscopy (DAS) is widely used for accurate measurement of temperature, gas concentration, and gas velocity in many areas, such as combustion diagnoses,[1–8] environmental monitoring, and chemical sensing.[9–14] The DAS technique is implemented by tuning the laser frequency over the selected absorption transition and acquiring the entire absorption feature. Particularly, by calculating the ratio of integrated absorbance at two transitions with distinct temperature dependence, temperature measurement can be realized, even in hostile environments where gas composition and pressure change rapidly with time.[3,4,6–8]

To acquire the entire features of the absorption transitions, a polynomial baseline fit to the non-absorbing wings of transmitted laser intensity is first performed to extrapolate incident laser intensity in the absorbing frequency region. Then, the absorbance is acquired by taking the ratio between the incident and transmitted laser intensity,[6,8] and the integrated absorbance can be obtained. However, the transmitted laser intensity is inevitably contaminated with background noise including laser intensity fluctuation, turbulent flow field-induced beam steering, interference signals from electric circuits, etc.[4,15] Therefore, raw experimental data of the absorbance extracted from the transmitted laser intensity is also contaminated with noise, which results in inaccurate calculation of the integrated absorbance, and hence erroneous inference of temperature and gas concentration. Fortunately, by fitting the absorbance features with lineshape functions, the influence of background noise can be reduced to a large extent in the DAS measurement. Furthermore, in case of the transitions superposed with small adjacent interference features, the transitions can be extracted from the adjacent interference features by using multi-peak lineshape fitting.[3,8,16] Therefore, it is necessary to fit the lineshape of the absorbance for DAS.

In general, the absorption features can be described by the Voigt lineshape which is the convolution of the two dominant broadening mechanisms which are collisional and Doppler, respectively.[6] Because the analytic form of Voigt function is unavailable, several numerical approaches were recently proposed to approximate the true Voigt function. For instance, Mendenhall computed the Voigt function via Fourier transform.[17] Dulov *et al.* obtained Voigt function by solving a parabolic partial differential equation.[18] However, the computation procedures in the mentioned approaches are rather complicated and resources-consuming, and hard to realize in a system-on-chip. However, in practical combustion scenarios such as coal-fired power plants[19] and incinerator facilities,[20] the temperature and gas concentrations should be measured *in situ* and in real time, in order to monitor the combustion efficiency and pollutant emissions on-line. Therefore, in this paper, we demonstrate a system-on-chip to fit the Voigt lineshape on-line in a real-time DAS measurement system.

## II. METHODOLOGY

The Voigt lineshape function is widely used for the calculation of spectral line profiles in the DAS measurement. Influenced by the simultaneous contribution of Gauss and Lorentz

a)Email: lijunxu@buaa.edu.cn

 

profiles, the Voigt lineshape function can be determined by both the Gauss and Lorentz FWHMs. However, the analytic form of Voigt lineshape function is unavailable. In the present work, a look-up table, which covers a range of combinations of Gauss and Lorentz FWHMs, was first built and Voigt lineshape was rapidly and accurately calculated by using interpolation. Then, with the look-up table and raw absorbance data in hand, Gauss-Newton nonlinear fitting module is implemented to obtain the parameters including both Gauss and Lorentz FWHMs, which can be used to calculate the integrated absorbance.

### A. Fundamentals of direct absorption spectroscopy

By calculating the integrated absorbance for the transitions, DAS provides an accurate and fast way for measuring the temperature and concentration along the laser path.[21] When a well collimated laser at central frequency $v$ [cm$^{-1}$] enters a gas sample with a total path length of $L$ [cm], a proportion of light is absorbed and the fractional transmission is described as

$$\left(\frac{I_t}{I_0}\right)_v = \exp\left(-P\int_0^L X_{abs}(x)S[T(x)]\phi_v dl\right), \quad (1)$$

where $I_t$ and $I_0$ are the transmitted and incident laser intensities, respectively. $P$ [atm] is the total pressure, $T(x)$ [K] is the local temperature, $X_{abs}(x)$ is the local mole fraction of the absorbing species, and $\phi_v$ [cm] is the lineshape function. The line strength of the transition, $S[T(x)]$ [cm$^{-2}$ atm$^{-1}$], is a function of the temperature shown as follows:

$$S(T) = S(T_0)\frac{Q(T_0)}{Q(T)}\left(\frac{T_0}{T}\right)\exp\left[-\frac{hcE''}{k}\left(\frac{1}{T}-\frac{1}{T_0}\right)\right] \times\left[1-\exp\left(\frac{-hcv_0}{kT}\right)\right]\left[1-\exp\left(\frac{-hcv_0}{kT_0}\right)\right]^{-1}, \quad (2)$$

where $h$ [J s] is Planck's constant, $c$ [cm s$^{-1}$] is the speed of light, $k$ [J K$^{-1}$] is Boltzmann's constant, $Q(T)$ is the partition function of the absorbing molecule given by HITRAN,[22] $T_0$ [K] is the reference temperature (usually 296 K), $v_0$ [cm$^{-1}$] is the line-center frequency, and $E''$ [cm$^{-1}$] is the lower energy of the transition.

The absorbance $\alpha_v$ is defined as

$$\alpha_v = -\ln\left(\frac{I_t}{I_0}\right)_v = \int_0^L X_{abs}(x)S[T(x)]\phi dl. \quad (3)$$

Because the lineshape function $\phi$ is normalized so that $\int_{-\infty}^{\infty}\phi dv \equiv 1$, the integrated absorbance $A$ of the transition, which is defined as the area underneath the absorption lineshape function, can be inferred from Eq. (3) as

$$A = \int_{-\infty}^{\infty}\alpha_v dv = \int_0^L X_{abs}(x)S[T(x)]dl. \quad (4)$$

Under the assumption of the same pressure, molar fraction, and path length of the laser beam, the ratio of the simultaneously measured $A$ of two transitions with different temperature dependence can be expressed as a function of the absorber temperature $T$ only, as indicated by Eq. (5),

$$R = \frac{A_1}{A_2} = \frac{S_1(T)}{S_2(T)} = \frac{S_1(T_0)}{S_2(T_0)}\exp\left[-\frac{hc(E_1'' - E_2'')}{k}\left(\frac{1}{T}-\frac{1}{T_0}\right)\right]. \quad (5)$$

Then, the average temperature along the laser path can be calculated as follows:

$$T = \frac{\frac{hc}{k}(E_2'' - E_1'')}{\ln\frac{A_1}{A_2} + \ln\frac{S_2(T_0)}{S_1(T_0)} + \frac{hc}{k}\frac{(E_2''-E_1'')}{T_0}}. \quad (6)$$

It should be mentioned that Eq. (6) is commonly used for temperature measurements along the laser path through a region of uniform temperature distribution. Then, the average molar fraction can be obtained from the integrated absorbance $A_1$ and the known $S_1(T)$,

$$X = \frac{A_1}{P\cdot S_1(T)\cdot L}. \quad (7)$$

### B. Fast calculation of Voigt lineshape function

In general, influenced by the combination of Doppler and collisional broadening mechanisms, the lineshape function $\phi$ can be expressed as convolution of a Gauss profile $\phi_G(v)$ and a Lorentz profile $\phi_L(v)$, noted as the Voigt lineshape function $\phi_V(v)$,[6]

$$\phi_V(v) = \int_{-\infty}^{+\infty}\phi_G(u)\cdot\phi_L(v-u)du. \quad (8)$$

The Gauss profile $\phi_G(v)$ and the Lorentz profile $\phi_L(v)$ can be expressed as follows:

$$\phi_G(v) = \frac{2}{w_G}\sqrt{\frac{\ln 2}{\pi}}\exp\left[-4\ln 2\left(\frac{v-v_0}{w_G}\right)^2\right], \quad (9)$$

$$\phi_L(v) = \frac{1}{2\pi}\frac{w_L}{(v-v_0)^2 + \left(\frac{w_L}{2}\right)^2}, \quad (10)$$

where $v_0$ [cm$^{-1}$] is the line center frequency, $w_G$ is the Gauss FWHM, $w_L$ is the Lorentz FWHM.

By defining a Voigt parameter $a$ as

$$a = \sqrt{\ln 2}\frac{w_L}{w_G}, \quad (11)$$

with the non-dimensional line position $w$ as

$$w = \frac{2\sqrt{\ln 2}(v-v_0)}{w_G}, \quad (12)$$

and the integral variable $y$ as

$$y = \frac{2u\sqrt{\ln 2}}{w_G}. \quad (13)$$

Then, the Voigt lineshape function is given by

$$\phi_V(v) = \frac{2}{w_G}\sqrt{\frac{\ln 2}{\pi}}\frac{a}{\pi}\int_{-\infty}^{+\infty}\frac{\exp(-y^2)}{a^2+(w-y)^2}dy. \quad (14)$$

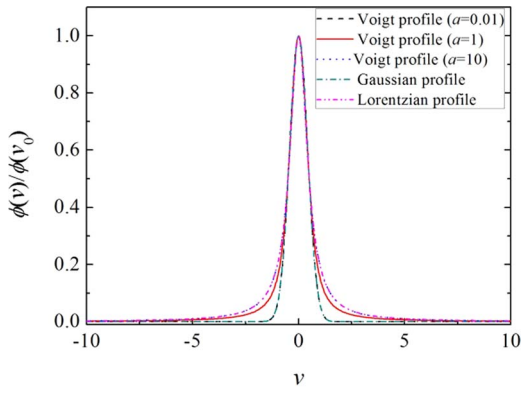


FIG. 1. Comparison of normalized Voigt lineshape with normalized Gaussian and Lorentzian lineshapes.

It is shown by Eq. (14) that although the analytic form of Voigt lineshape function is unavailable, it can be solely determined by a combination of $w_G$ and $w_L$. As shown by Eqs. (11) and (12), both $w_G$ and $w_L$ are functions of $a$ and $w$. It should be noted that the Voigt parameter $a$ describes the profile of the lineshape. It can be seen from Figure 1 that, when $a \geq 10$, the Voigt profile becomes a Lorentzian profile, while that becomes a Gaussian profile for $a \leq 0.01$. Therefore, Eq. (14) can be expressed by Eqs. (15) and (16) for simplicity in case of $a \geq 10$ and $a \leq 0.01$, respectively,

$$\phi_V(v) = \frac{2}{w_G}\sqrt{\frac{\ln 2}{\pi}}\frac{1}{\sqrt{\pi}}\left(\frac{a}{a^2+w^2}\right) \quad \text{for } a \geq 10, \tag{15}$$

$$\phi_V(v) = \frac{2}{w_G}\sqrt{\frac{\ln 2}{\pi}}e^{-w^2} \quad \text{for } a \leq 0.01. \tag{16}$$

In case of $0.01 \leq a \leq 10$, each combination of $a$ and $w$ determines a point in the Voigt profile. In general, different points on the Voigt profile can be obtained by calling an identical value of $a$, but different values of $w$. Given a value of $a$, $\phi_V(v)$ infinitely approaches zero as $w$ increases. To save storage space, if a value of $w$ for each value of $a$ makes $\phi_V(v)/\phi_V(v_0) < 0.005$, the value of $w$ is ignored. Therefore, a look-up table, which depends on $a$ and $w$, was built in this work, as shown in Figure 2 and Table I. It should also be noted

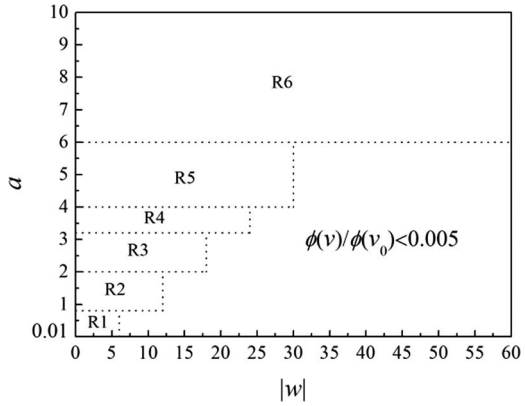


FIG. 2. Approximation regions of the Voigt lineshape function for $0.01 \leq a \leq 10$.

TABLE I. The boundaries between the approximation regions and the step sizes of $a$ in each approximation region in Figure 2.

| Regions | Boundaries | Step sizes of $w$ | Step sizes of $a$ |
|---|---|---|---|
| 1 | $0 \leq \|w\| < 6$, $0.01 \leq a < 0.8$ | 0.01 | 0.005 |
| 2 | $0 \leq \|w\| \leq 12$, $0.8 \leq a < 2$ | 0.02 | 0.01 |
| 3 | $0 \leq \|w\| \leq 18$, $2 \leq a < 3.2$ | 0.03 | 0.015 |
| 4 | $0 \leq \|w\| \leq 24$, $3.2 \leq a < 4$ | 0.04 | 0.02 |
| 5 | $0 \leq \|w\| \leq 30$, $4 \leq a < 6$ | 0.05 | 0.025 |
| 6 | $0 \leq \|w\| \leq 60$, $6 \leq a \leq 10$ | 0.1 | 0.05 |

that the step sizes of $a$ and $w$ in the approximation regions are varied to meet the requirement of accuracy, which will be discussed in Sec. IV. With $a$ and $w$ in hand, pre-computed points over a Voigt profile can be obtained by specifying the grid of $w$ values and the single $a$ value. By interpolating between the pre-computed points, the Voigt profile can be rapidly and accurately calculated,[23] as shown in Figure 3. By subtracting the calculated Voigt lineshape from the "true" value, which is calculated from Matlab calculation, absolute error $|\varepsilon|$ can be obtained, which is shown in the upper panel of Figure 3. To examine the accuracy of the proposed algorithm for all the approximation regions, absolute errors $|\varepsilon|$ for $0.01 \leq a \leq 10$ are obtained, as shown in Figure 4. The values of $|\varepsilon|$ are consistently smaller than $1.5 \times 10^{-4}$. In detail, 99.996% values of $|\varepsilon|$ are smaller than $10^{-4}$, while 93.8% of those are smaller than $10^{-5}$.

### C. Voigt lineshape fitting

According to Eqs. (3) and (4), the absorbance $\alpha_v$ can be represented by the product of the integrated absorbance $A$ and the Voigt lineshape function $\phi_v(v)$,

$$\alpha_v(v) = A \cdot \phi_V(v) = A \cdot \frac{2}{w_G}\sqrt{\frac{\ln 2}{\pi}}\frac{a}{\pi}\int_{-\infty}^{+\infty}\frac{\exp(-y^2)}{a^2+(w-y)^2}dy. \tag{17}$$

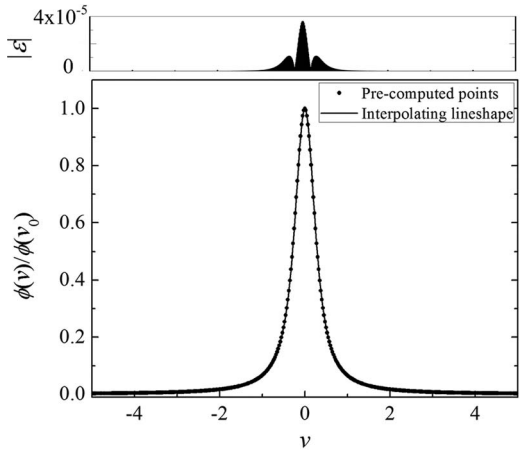


FIG. 3. The pre-computed points and the interpolated Voigt lineshape for $a = 2$. The absolute errors between the interpolated Voigt lineshape and the true values are shown above the figure.

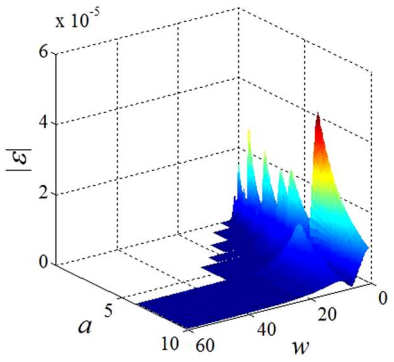


FIG. 4. Absolute error between the Voigt lineshape calculated from the look-up table and the true value for $0.01 \le a \le 10$.

Therefore, a nonlinear fitting model can be established as follows:

$$f(\mathrm{x}, t) = f(x_1, x_2, x_3, t) = x_1 \int_{-\infty}^{+\infty} \frac{x_3 e^{-y^2}}{(x_2 t - y)^2 + {x_3}^2} dy, \tag{18}$$

where $f(\mathrm{x}, t) = \alpha_v$, $t = v - v_0$, and x the fitting parameters:

$$\mathrm{x} = \begin{pmatrix} x_1 \\ x_2 \\ x_3 \end{pmatrix} = \begin{pmatrix} A\frac{2\sqrt{\ln 2}}{\pi^{3/2} w_G} \\ \frac{2\sqrt{\ln 2}}{w_G} \\ \sqrt{\ln 2}\frac{w_L}{w_G} \end{pmatrix}. \tag{19}$$

The flow diagram of Voigt fitting process is shown in Figure 5. First, the initial values of the fitting parameters are set. By directly integrating the raw absorbance $\alpha_v'$, the initial value of the integrated absorbance $A_{init}$ can be obtained. Furthermore, a coarse FWHM $w_{init}$ can be obtained from the raw absorbance. By setting $w_{init} = w_G = w_L$, the initial values of the fitting parameters $\mathrm{x}_{init}$ can be obtained from Eq. (19). Then, given the measured absorbance $\alpha_v'$ and $f(\mathrm{x}, t)$ calculated from the look-up table, the fitting parameters can be obtained by minimizing $\|f(\mathrm{x}, t) - \alpha_v'\|^2$, noted as $\|\varepsilon(\mathrm{x}, t)\|^2$, or equivalently finding

$$\mathrm{x}^* = \arg\min_{\mathrm{x}} \{F(\mathrm{x})\}, \tag{20}$$

where

$$F(\mathrm{x}) = \frac{1}{2}\|\varepsilon(\mathrm{x}, t)\|^2 = \frac{1}{2}\varepsilon(\mathrm{x}, t)^{\mathrm{T}}\varepsilon(\mathrm{x}, t), \tag{21}$$

$\mathrm{X} \in \mathbf{R}^{n\times 1}$, $\alpha_v'$, $t$, $\varepsilon(\mathrm{x}, t)$, $f(\mathrm{x}, t) \in \mathbf{R}^{m\times 1}$, $m$ is the number of data points $(t_1, f(\mathrm{x}, t_1))$, $(t_2, f(\mathrm{x}, t_2))$, …, $(t_m, f(\mathrm{x}, t_m))$, $n$ is the number of fitting parameters, i.e., $n = 3$ in this case. Given by Eq. (19), the integral of the integrated absorbance $A$ is calculated from $x_1$ and $x_2$, and the accuracy of $A$ improves while iterating. The iterations stop when either the maximum number of iterations $N_{\max}$ or the relative difference of the integrated absorbance at the $i$th iteration $\Delta A(i)$ reaches 20 and 5 $\times 10^{-3}$, respectively. $\Delta A(i)$ is defined as

$$\Delta A(i) = \frac{|A(i+1) - A(i)|}{A(i)}. \tag{22}$$

To solve the nonlinear least square problem, Gauss-Newton method is used,[24] which is based on a linear approximation to the components of $\varepsilon(\mathrm{x}, t)$ in the neighborhood of x.

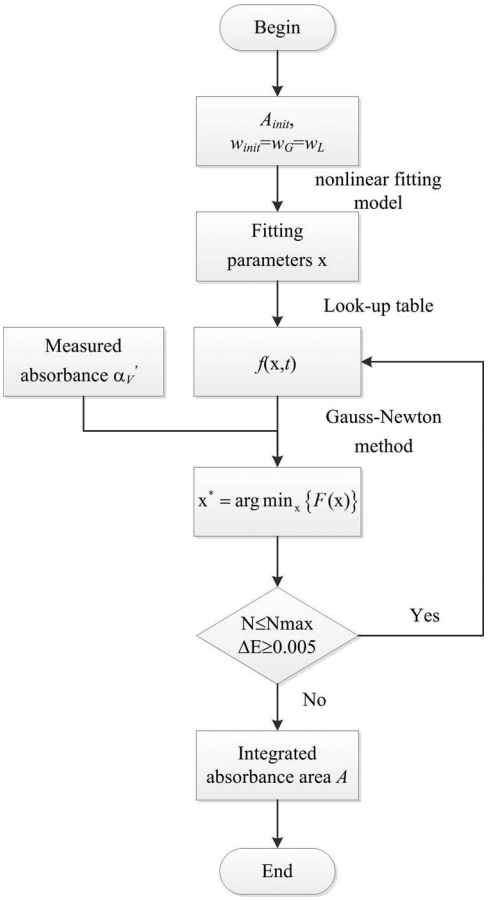


FIG. 5. Flow diagram of Voigt fitting process.

for small $\|h\|$, he Taylor expansion of $\varepsilon(\mathrm{x}, t)$ is expressed as

$$\varepsilon(\mathrm{x} + \mathrm{h}) \approx l(h) = \varepsilon(\mathrm{x}) + \mathrm{J}(\mathrm{x})\mathrm{h}, \tag{23}$$

where $\mathrm{J} \in \mathbf{R}^{m\times n}$ is the Jacobian. This is a matrix containing the first partial derivatives of $\varepsilon(\mathrm{x}, t)$,

$$(\mathrm{J}(\mathrm{x}))_{ij} = \frac{\partial \varepsilon_i(\mathrm{x})}{\partial x_j}, \quad i = 1, 2, \ldots, m, \quad j = 1, 2, \ldots, n. \tag{24}$$

Therefore, we can obtained Eq. (25) from Eqs. (21) and (24) that

$$\frac{\partial F(\mathrm{x})}{\partial x_j} = \sum_{i=1}^{m} \varepsilon_i(\mathrm{x}) \frac{\partial \varepsilon_i(\mathrm{x})}{\partial x_j}, \quad \text{or } F'(\mathrm{x}) = \mathrm{J}(\mathrm{x})^{\mathrm{T}}\varepsilon(\mathrm{x}). \tag{25}$$

Inserting Eq. (23) to Eq. (21),

$$\begin{aligned} F(\mathrm{x} + \mathrm{h}) \approx L(\mathrm{h}) &= \frac{1}{2} l(\mathrm{h})^{\mathrm{T}} l(\mathrm{h}) \\ &= \frac{1}{2}\varepsilon^{\mathrm{T}}\varepsilon + \mathrm{h}^{\mathrm{T}}\mathrm{J}^{\mathrm{T}}\varepsilon + \frac{1}{2}\mathrm{h}^{\mathrm{T}}\mathrm{J}^{\mathrm{T}}\mathrm{J}\mathrm{h} \\ &= F(\mathrm{x}) + \mathrm{h}^{\mathrm{T}}\mathrm{J}^{\mathrm{T}}\varepsilon + \frac{1}{2}\mathrm{h}^{\mathrm{T}}\mathrm{J}^{\mathrm{T}}\mathrm{J}\mathrm{h}. \end{aligned} \tag{26}$$

The Gauss-Newton step $\mathrm{h}_{\mathrm{gn}}$ minimizes $L(\mathrm{h})$,

$$\mathrm{h}_{\mathrm{gn}} = \arg\min_{\mathrm{h}} \{L(\mathrm{h})\}. \tag{27}$$

TABLE II. Two $H_2O$ absorption transitions selected for the experiment.

| Transition index | Frequency $v_0$ ($cm^{-1}$) | $S$ at 296 K ($cm^{-2}$ $atm^{-1}$) | $E''$ ($cm^{-1}$) |
|---|---|---|---|
| 1 | 7444.35 + 7444.37 combined | $1.10 \times 10^{-3}$ | 1774.75<br>1806.67 |
| 2 | 7185.6 | $1.96 \times 10^{-2}$ | 1045.058 |

The gradient of $L(\mathrm{h})$ are

$$L'(\mathrm{h}) = \mathrm{J}^{\mathrm{T}}\varepsilon + \mathrm{J}^{\mathrm{T}}\mathrm{J}\mathrm{h}, \tag{28}$$

$$L''(\mathrm{h}) = \mathrm{J}^{\mathrm{T}}\mathrm{J}. \tag{29}$$

Comparing Eqs. (25) and (28), it can be deduced that $L'(0) = F'(\mathrm{x})$. Furthermore, it can be seen from Eq. (29) that $L''(\mathrm{h})$ is independent of h. $L''(\mathrm{h})$ is symmetric and if J has full rank, then $L''(\mathrm{h})$ is also positive definite. In this way, $L(\mathrm{h})$ has a unique minimizer, which can be found by solving

$$\begin{aligned}(\mathrm{J}^{\mathrm{T}}\mathrm{J})\mathrm{h}_{\mathrm{gn}} &= -\mathrm{J}^{\mathrm{T}}\varepsilon,\\ \mathrm{x}_{i+1} &= \mathrm{x}_i + \mathrm{h}_{\mathrm{gn}_i}.\end{aligned} \tag{30}$$

## III. RESULTS AND DISCUSSIONS

### A. Line selection

As a major product of the combustion of hydrocarbons, water vapor ($H_2O$) has a rich spectrum in the readily accessible near-infrared spectrum range of communication-grade tunable diode lasers. Therefore, $H_2O$ was selected as the target absorbing species in the experiment. According to the criteria of line selection,[3,15,16] two main criteria were used to select two transitions in this work. First, the absorption strength should be moderate. Too large absorption strength will lead to a too small signal in the detector, whereas too small absorption strength will not be differentiated by the detector. Second, suitable lower state energy $E''$ should be provided to ensure high sensitivity in the temperature range in the work. To satisfy the above criteria, the $H_2O$ transitions of 7444.36 $cm^{-1}$ (7444.35 $cm^{-1}$ combined with 7444.37 $cm^{-1}$) and 7185.6 $cm^{-1}$, which can be accessed by the distributed feedback diode (DFB) lasers available in our laboratory, were used in the experiment, as shown in Table II. It should be noted that the lineshape of the different transitions can be universally regarded as the Voigt lineshape. Because the method is proposed and implemented to on-line fit the Voigt lineshape, it is suitable for other gas species.

### B. Experiments and results

#### 1. Experimental system

As shown in Figure 6, the experimental system consists of two DFB lasers with line-width of 10 MHz and output power of 10 mW, each controlled independently by a laser diode controller. The laser diode controller provides temperature and current control for the DFB lasers. The current of both controllers was simultaneously modulated by a ramp signal from a double-channel function generator, so that the wavelengths of the DFB lasers can be scanned within a spectral range of ~1.5 $cm^{-1}$ around the central wavelengths. Subsequently, a 2 × 2 fiber-coupler splits the laser into two channels. The laser in the first channel is collimated and delivered into a solid etalon with a free spectral range of 2.53 GHz to monitor the frequency during the wavelength scanning. The laser in the second channel is collimated and penetrates the target flame generated by a McKenna flat flame burner, which is widely used as calibration source for combustion research.[25,26] By shielding the burner plate with nitrogen, a laminar flame with uniform temperature and $H_2O$ concentration distribution above the burner plate can be obtained. Furthermore, different values of temperature and $H_2O$ concentration can also be obtained by adjusting the equivalent ratio of the premixed propane/air fuel. Finally, the optical signals are converted to voltage signals by the photodiode detectors, which are connected with data acquisition and processing circuits. To eliminate the interference absorption by $H_2O$ vapor in room air, the open paths in the second channel are protected by two stretchable pipes, which are filled with nitrogen, as shown in Figure 7. By adjusting the lengths of the stretchable pipes, the laser path except the flame region can be purged with nitrogen.

Two absorption signals were obtained by using a time division multiplexing scheme.[16] In detail, the laser scanning rate is 5 kHz. During a scanning period, the current was set under the lower working threshold of the DFB laser for 0.05 ms and was scanned by the ramp signal for 0.15 ms. The phase difference of the double-channel scanning signals was 180°. By combining the two lasers with a single mode 2 × 2 fiber-couplers, the absorption signals for the two transitions in Table II can be obtained within 0.4 ms, as shown

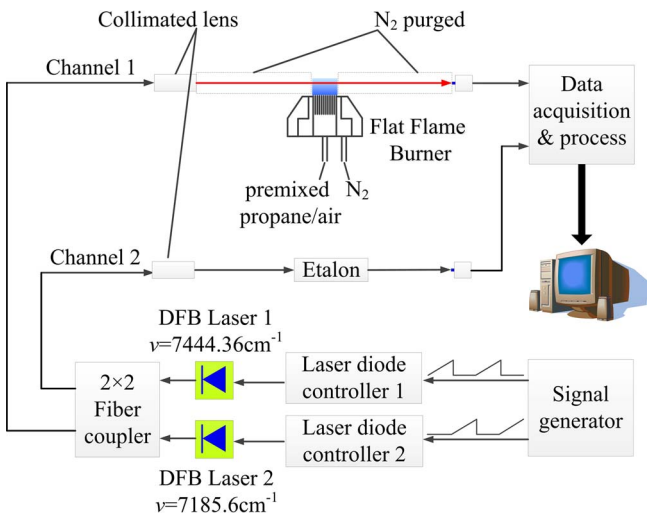


FIG. 6. Schematic of the direct absorption spectroscopy system.

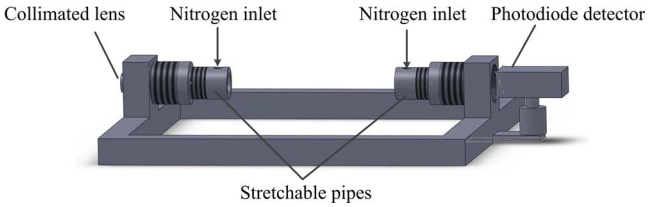


FIG. 7. Optical sensors in the direct absorption spectroscopy system.

in Figure 8. To yield a background signal and correct the combustion emission, a further 0.1 ms is required to set the current underneath the lower working limit of the threshold.

In the data acquisition and processing circuits, the voltage signals of two channels are simultaneously sampled by a dual 12-bit analog to digital converter (ADC, AD7356, Analog Devices) with 5 Mega samples per second (MSPS) per channel. To fit the Voigt lineshape on-line and calculate the integrated absorbance for two transitions, a floating-point digital signal processor (DSP, TMS320C6713B, Texas Instruments) is employed, which works with 200 MHz clock rates. Furthermore, a USB Microcontroller (CY7C68013, Cypress) is used in the data acquisition and processing circuits to communicate with computer. As the central processing unit in the data acquisition and processing circuits, a field programmable gate array (FPGA, EP2C8F256C8, Altera), which works with 50 MHz, are implemented to provide parallel sequential logic control to the ADC, DSP, and USB, as shown in Figure 9.

### 2. Experimental results

As discussed in Sec. III B, the current of the DFB lasers was scanned by the ramp signal for 0.15 ms within a scanning period. Therefore, a total of 750 points are obtained by the FPGA within the ramp scan because the ADC is of 5 MSPS. As shown in Figure 9(a), the FPGA communicates with the DSP through multichannel buffered serial ports (McBSP). However, constrained to the data transferring speed of the McBSP, all 750 points are unable to be transferred from the FPGA to the DSP within 0.15 ms in order to fit the Voigt lineshape on-line. Therefore, the FPGA is used to pre-process the absorption signals shown in Figure 8 and select necessary points for Voigt lineshape fitting. First, for two non-absorption regions, a median filter is implemented to reduce the influence

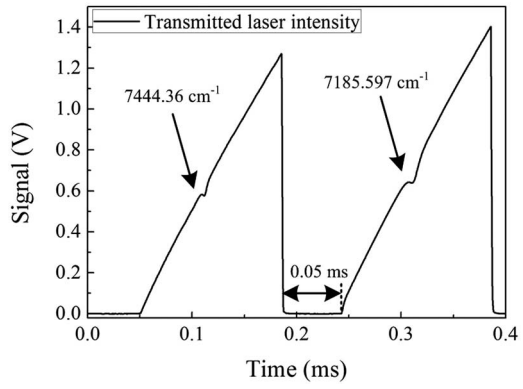


FIG. 8. Signal of transmitted laser intensity obtained by the TDM scheme.

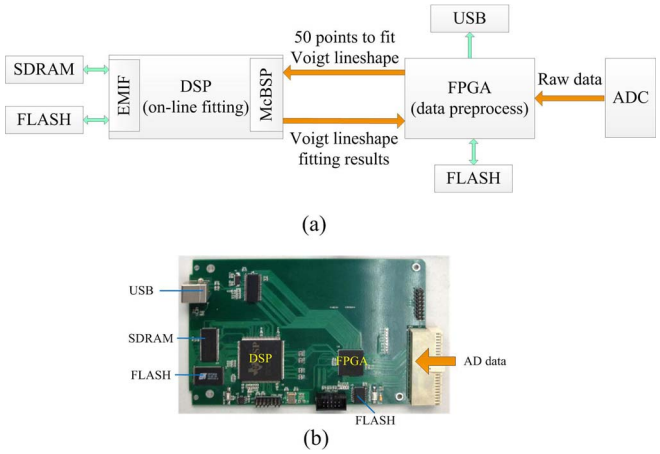


FIG. 9. Data acquisition and processing circuit. (a) Schematic diagram and (b) photography of the circuit.

of background noise. Second, 5 equally spaced points on each the non-absorption region, a total of 10 points, which are used to fit the baseline by the DSP, are selected and transferred from the FPGA to the DSP through the McBSP, as shown in Figure 10. Third, by obtaining first-order difference of the absorption signals, the point of the absorbance peak can be found. The point, whose value closest to the mean value of the first-order difference of the absorption signals, is corresponded to the peak of the absorbance. As shown in Figure 10, in case of the transition $v = 7444.36\ \mathrm{cm}^{-1}$, because small interference transitions exist on the left wing of the absorbance, 10 points from the peak of the absorbance to the left wing and 30 points from the peak to the end of the right wing are used to fit the Voigt lineshape, which are also transferred from the FPGA to the DSP through the McBSP. It should be noted that transferring a total of 50 points through the McBSP consumes approximately 0.05 ms if the FPGA works with 50 MHz clock rates, which satisfies on-line Voigt lineshape fitting.

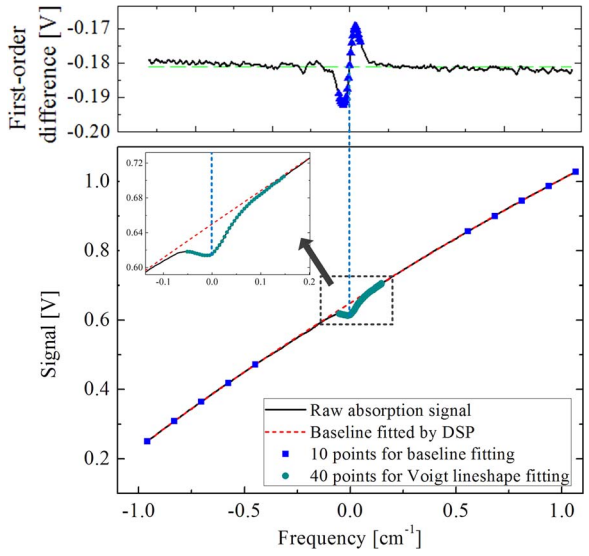


FIG. 10. The raw absorption signal and the selected 50 points that were fed to the DSP through the McBSP of the transition $v = 7444.36\ \mathrm{cm}^{-1}$. In detail, 10 points are selected for baseline fitting, while 40 points are selected for Voigt lineshape fitting by the DSP.

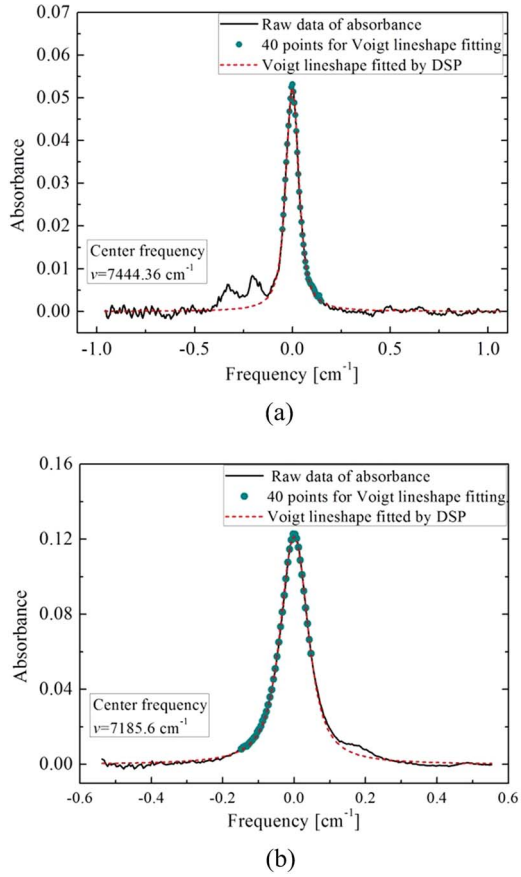


FIG. 11. The Voigt lineshapes on-line fitted by DSP for the transitions (a) $v = 7444.36\ \text{cm}^{-1}$ and (b) $v = 7185.6\ \text{cm}^{-1}$, respectively.

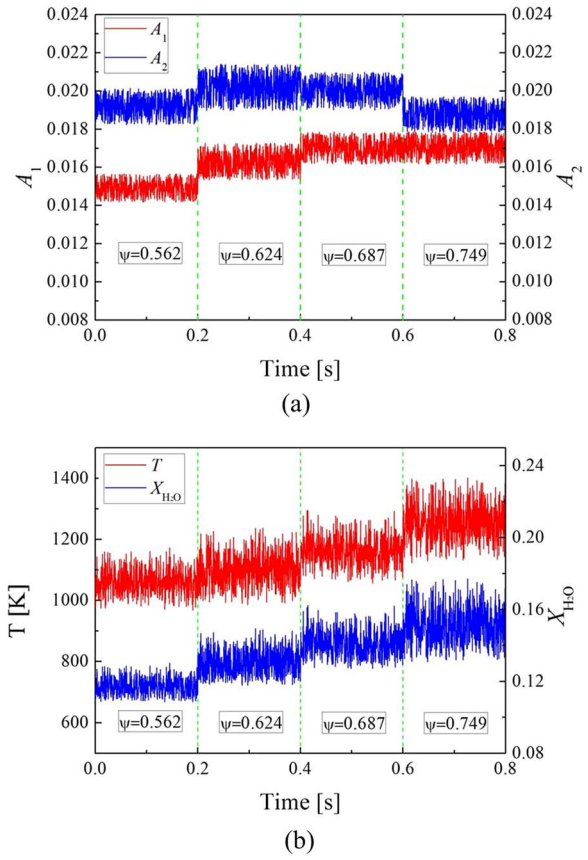


FIG. 12. Measurement results obtained by the DSP-based on-line Voigt lineshape fitting. (a) The integrated absorbance for the transitions of 7444.36 $\text{cm}^{-1}$ and 7185.6 $\text{cm}^{-1}$, $A_1$ and $A_2$, when the equivalent ratio $\psi$ was set as 0.562, 0.624, 0.687, and 0.749 in sequence for every 200 ms. (b) Temperature $T$ and $H_2O$ concentration $X_{H2O}$ retrieved by the DSP-based on-line Voigt fitting for each equivalent ratio in Figure 12(a).

The DSP used the 50 points to on-line fit the Voigt lineshape. First, by using a 3-order polynomial, the baseline can be fitted by the DSP and thus the absorbance can be further obtained, as shown in Figure 11. Second, as discussed in Sec. II B, to rapidly and accurately calculate the Voigt lineshape, the look-up table, with size of 1.3 MB, was built for $0.01 \le a \le 10$ and $|w| \le 10$. The look-up table was stored and called by FLASH and SDRAM through external memory interface (EMIF) of the DSP, respectively. Third, with the look-up table and the 50 points of the absorbance in hand, Gauss-Newton nonlinear fitting, as discussed in Sec. II C, was used to obtain the fitting parameters containing Gauss and Lorentz FWHMs in Eq. (19). Finally, the fitting parameters were transferred from the DSP to the FPGA through the McBSP. By connecting USB with a computer, the fitting parameters were transferred from FPGA to a computer through USB, and the integrated absorbance, as well as the Gauss and Lorentz FWHMs were calculated by the computer. With the Gauss and Lorentz FWHMs in hand, the Voigt lineshape can be obtained, as shown in Figure 11(a). Similar data pre-process strategy and fitting method are also suitable for the transition of 7185.6 $\text{cm}^{-1}$, as shown in Figure 11(b).

In the experiment, the flow of the air was set as 15.25 l/min, while the flow of the propane was set as 0.9, 1.0, 1.1, 1.2 l/min in sequence for every 200 ms, i.e., the equivalent ratio of the premixed propane/air fuel was set as 0.562, 0.624, 0.687, and 0.749 in sequence. As shown in Figure 12(a), by sampling the data for 0.8 s and using the DSP-based on-line Voigt fitting, we can obtain the integrated absorbance for the transitions of 7444.36 $\text{cm}^{-1}$ and 7185.6 $\text{cm}^{-1}$ for each equivalent ratio, $A_1$ and $A_2$, respectively. Then, the temperature can be retrieved by using Eq. (6) for each equivalent ratio. With the temperature $T$ in hand, the value of $H_2O$ concentration $X_{H2O}$ corresponding to each value of $T$ can be obtained by using Eq. (7), as shown in Figure 12(b).

To evaluate the performance of the proposed method and the hardware design, the expected $T$ and $X_{H2O}$ of the McKenna flat flame burner are compared with those retrieved by the DSP-based on-line Voigt fitting. To quantitatively measure the expected $T$ of the flame, an S-type thermocouple was employed, which was mounted adjacent to the path that the laser beam passes through. Then, $X_{H2O}$ can be obtained from equilibrium calculations. Furthermore, $T$ and $X_{H2O}$ retrieved by the DSP-based on-line Voigt fitting were also compared with those obtained from on-line integral of the raw absorbance. Because small adjacent interference transitions always exist on a wing of the lineshape, the integral of the raw absorbance can be calculated by integrating the absorbance from the peak to the end of the wing on the side without interference transitions. For instance, as shown in Figure 11(a), for the

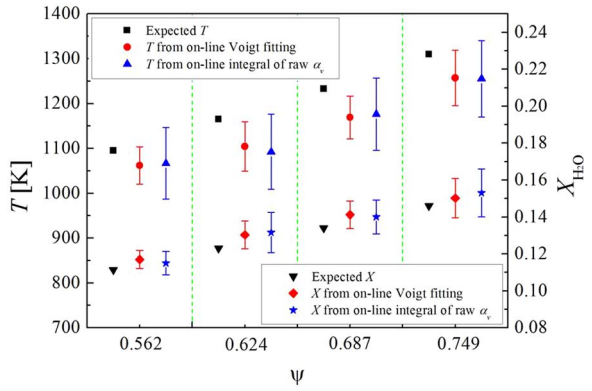


FIG. 13. Mean values with their standard deviations of $T$ and $X_{H2O}$ retrieved by using DSP-based on-line Voigt fitting and on-line integral of the raw absorbance for the equivalent ratio of 0.562, 0.624, 0.687, and 0.749, respectively.

transition of 7444.36 $cm^{-1}$, small interference transitions exist on the left wing of the lineshape. Therefore, the on-line integral of the raw absorbance was calculated from $v = 0$ to 0.8 $cm^{-1}$.

The retrieved temperature and $H_2O$ concentration with their standard deviations (STDs) were shown in a bin for each equivalent ratio. As shown in Figure 13, the midpoint signifies the mean of the solutions of $T$ and $X_{H2O}$ for each equivalent ratio, and the error bar to each midpoint denotes the STD of the solutions. To prevent the error bars from overlapping and increase the visibility of Figure 13, we separated the error bars from each other in the bin. For each equivalent ratio, it can be seen that the standard deviations of $T$ and $X_{H2O}$ obtained by the DSP-based on-line Voigt fitting are smaller than those from on-line integral of the raw absorbance, denoting that the proposed method and hardware are more precise and necessary to be adopted in the real-time DAS system. In other words, when using the on-line Voigt lineshape fitting, the measurement results are less sensitive to background noise that superposing on absorbance signal. It can be seen from Figure 13 that the retrieved mean values of $T$ are smaller than the expected values for each equivalent ratio. This is mainly caused by radiation loss from the flame to the surroundings and the heat conduction to the water-cooled burner surface. Furthermore, in the DAS system, only the flat flame above the burner plate is desired and the open paths in the laser path are purged with nitrogen, in order to eliminate the interference absorption by $H_2O$ vapor in room air. However, the room air, normally with $X_{H2O}$ of 1%–2%, is inevitably enclosed in the laser path at the edge of the flow fields. Therefore, it can also be seen from Figure 13 that the mean values of the retrieved $X_{H2O}$ are slightly larger than the expected values. It should be noted that by measuring multiple transitions of $H_2O$, the influence of the radiation loss and the room air on the measurement results can be reduced to a large extent.[1,27–29]

### C. Discussions

As discussed in Sec. II B, the step sizes of $a$ and $w$ in the approximation regions, illustrated in Figure 2 and Table I, are varied to meet the accuracy requirements. Furthermore, to save storage space, the values of $w$ leading to $\phi_v(v)/\phi_v(v_0) < 0.005$ are ignored for each value of $a$ in this work. With the selected step sizes and boundaries of $a$ and $w$, the 1.3 MB look-up table was established, which was stored in the FLASH and called by the SDRAM through external memory interface of the DSP. As shown in Figure 3(b), the maximum absolute errors $|\varepsilon|$ between the true Voigt lineshape and that calculated by the look-up table is $1.5 \times 10^{-4}$. As given in Sec. III B, the ADC adopted in the experiment is of 12 bits, therefore, the resolution of the data acquisition and processing circuits is $1/2^{12}$ ($1/2^{12} = 2.44 \times 10^{-4}$). Obviously, $|\varepsilon|$ is smaller than the resolution of ADC. That is to say, even though the look-up table is of much smaller step size and wider range of $a$ and $w$, the fitted Voigt lineshape of higher accuracy cannot be differentiated by the 12-bit ADC. Therefore, the selected step sizes and boundaries of $a$ and $w$ are sufficient to meet the accuracy requirements in the work. It should be noted that $|\varepsilon|$ describes the accuracy of the established model. If the ADC of the data acquisition and processing circuits is of higher resolution, smaller step size and wider range of $a$ and $w$ are required.

It should also be noted that the maximum number of iterations $N_{max}$ is determined by processing speed of the DSP. Generally, it costs the DSP about 0.01 ms for each iteration. As shown in Figure 8, the laser scanning rate is 5 kHz, that is to say, the DSP will not able to fit the next Voigt lineshape if the number of iteration exceeds 20. Therefore, $N_{max}$ was set to 20 in the experiment. The relative difference of the integrated absorbance between two adjacent iterations $\Delta A$ is determined by the level of DAS measurement noise in the experiment. As shown in Figure 12(a), compared with the relative measurement noise, i.e., around 7% in the experiment, the relative difference of $A$ $5 \times 10^{-3}$ is sufficiently small. To guarantee the accuracy of the DAS measurement, $|\varepsilon|$ should be significantly smaller than $\Delta A$. Generally, if $|\varepsilon|$ is significantly smaller than $\Delta A/10$, the fitting error caused by the limited size of the look-up table can be neglected. In the experiment, $|\varepsilon|$ is smaller than $\Delta A/30$, it can be assumed that the selected size of the look-up table has no impact on the measurement accuracy. Furthermore, $\Delta A$ is also determined by the processing speed of the DSP. Smaller $\Delta A$ will result in more iterations and longer calculation time. If the signal to noise ratio of the DAS measurement is larger and the processor is faster than those in the experiment, $\Delta A$ could be set smaller to obtain more accurate fitting results.

## IV. CONCLUSIONS

To the best of the authors' knowledge, this is the first report of high-precision on-line Voigt lineshape fitting for real-time DAS measurement in a system-on-chip, i.e., a digital signal processor, in this paper. First, a look-up table, which covers a range of combinations of the Gauss and Lorentz FWHMs, was first established and stored in the FLASH of the DSP and the Voigt lineshape was rapidly and accurately calculated by interpolation. Second, a 12 bit ADC was used to sample the absorption signal with 5 MHz in the experiment. The absorption signal was pre-processed by the FPGA,

in which 50 points in the raw experimental data are selected and fed to the DSP to fit the baseline and the Voigt lineshape. Finally, with the look-up table and the 50 points in hand, Gauss-Newton nonlinear fitting was implemented by the DSP to obtain the fitting parameters including both the Gauss and Lorentz FWHMs, which can be used to calculate the integrated absorbance.

In the real-time DAS experiment, the temperature and $H_2O$ concentration of a McKenna flat flame burner were obtained on-line by calculating the transitions of 7444.36 $cm^{-1}$ and 7185.6 $cm^{-1}$ with the DSP-based on-line Voigt lineshape fitting and on-line integral of the raw absorbance, respectively. For different equivalent ratio of the premixed propane/air fuel, temperature and $H_2O$ concentration retrieved by using the proposed method and hardware are less sensitive to the background noise compared with those from on-line integral of the raw absorbance.

## ACKNOWLEDGMENTS

The authors gratefully acknowledge the financial support by the National Science Foundation of China (Grant Nos. 61225006, 61327011, and 61311201), Beijing Higher Education Young Elite Teacher Project (YETP1134), and the Fundamental Research Funds for the Central Universities (Grant Nos. YWF-14-YJSY-042 and YWF-10-03-044).

[1]C. Liu, L. Xu, and Z. Cao, "Measurement of nonuniform temperature and concentration distributions by combining line-of-sight TDLAS with regularization methods," Appl. Opt. **52**, 4827–4842 (2013).
[2]O. Witzel, A. Klein, S. Wagner, C. Meffert, C. Schulz, and V. Ebert, "High-speed tunable diode laser absorption spectroscopy for sampling-free in-cylinder water vapor concentration measurements in an optical IC engine," Appl. Phys. B **109**, 521–532 (2012).
[3]F. Li, X. Yu, H. Gu, Z. Li, Y. Zhao, L. Ma *et al.*, "Simultaneous measurements of multiple flow parameters for scramjet characterization using tunable diode-laser sensors," Appl. Opt. **50**, 6697–6707 (2011).
[4]S. Li, A. Farooq, and R. K. Hanson, "$H_2O$ temperature sensor for low-pressure flames using tunable diode laser absorption near 2.9 $\mu$m," Meas. Sci. Technol. **22**, 125301–125311 (2011).
[5]A. Farooq, J. B. Jeffries, and R. K. Hanson, "*In situ* combustion measurements of $H_2O$ and temperature near 2.5 $\mu$m using tunable diode laser absorption," Meas. Sci. Technol. **19**, 075604 (2008).
[6]X. Liu, "Line-of-sight absorption of $H_2O$ vapor: Gas temperature sensing in uniform and nonuniform flows," Ph.D. dissertation (Department of Mechanical Engineering, Stanford University, 2006).
[7]X. Liu, J. B. Jeffries, R. K. Hanson, K. M. Hinckley, and M. A. Woodmansee, "Development of a tunable diode laser sensor for measurements of gas turbine exhaust temperature," Appl. Phys. B: Lasers Opt. **82**, 469–478 (2006).
[8]K. Sun, S. Wang, R. Sur, X. Chao, J. B. Jeffries, and R. K. Hanson, "Sensitive and rapid laser diagnostic for shock tube kinetics studies using cavity-enhanced absorption spectroscopy," Opt. Express **22**, 9291–9300 (2014).
[9]M. B. Frish, R. T. Wainner, M. C. Laderer, B. D. Green, and M. G. Allen, "Standoff and miniature chemical vapor detectors based on tunable diode laser absorption spectroscopy," IEEE Sens. J. **10**, 639–646 (2010).
[10]S. Pal and H. McCann, "Auto-digital gain balancing: A new detection scheme for high-speed chemical species tomography of minor constituents," Meas. Sci. Technol. **22**, 115304 (2011).
[11]P. Wright, N. Terzija, J. L. Davidson, S. Garcia-Castillo, C. Garcia-Stewart, S. Pegrum *et al.*, "High-speed chemical species tomography in a multi-cylinder automotive engine," Chem. Eng. J. **158**, 2–10 (2010).
[12]C. F. Kaminski, R. S. Watt, A. D. Elder, J. H. Frank, and J. Hult, "Supercontinuum radiation for applications in chemical sensing and microscopy," Appl. Phys. B: Lasers Opt. **92**, 367–378 (2008).
[13]X. Zhou, X. Liu, J. B. Jeffries, and R. K. Hanson, "Development of a sensor for temperature and water concentration in combustion gases using a single tunable diode laser," Meas. Sci. Technol. **14**, 1459–1468 (2003).
[14]Q. Huang, F. Wang, H. Zhang, J. Yan, M. Ni, and K. Cen, "In-situ CO measurement of gas and oil combustion flame using near infrared tunable diode laser with direct and modulated absorption signals," Opt. Commun. **306**, 99–105 (2013).
[15]J. T. C. Liu, G. B. Rieker, J. B. Jeffries, M. R. Gruber, C. D. Carter, T. Mathur, and R. K. Hanson, "Near-infrared diode laser absorption diagnostic for temperature and water vapor in a scramjet combustor," Appl. Opt. **44**, 6701–6711 (2005).
[16]C. Liu, L. Xu, Z. Cao, and H. McCann, "Reconstruction of axisymmetric temperature and gas concentration distributions by combining fan-beam TDLAS with onion-peeling deconvolution," IEEE Trans. Instrum. Meas. **63**, 3067–3075 (2014).
[17]M. H. Mendenhall, "Fast computation of Voigt functions via Fourier transforms," J. Quant. Spectrosc. Radiat. Transfer **105**, 519–524 (2007).
[18]E. N. Dulov and D. M. Khripunov, "Voigt lineshape function as a solution of the parabolic partial differential equation," J. Quant. Spectrosc. Radiat. Transfer **107**, 421–428 (2007).
[19]X. Chao, J. Jeffries, and R. Hanson, "Real-time, in situ, continuous monitoring of CO in a pulverized-coal-fired power plant with a 2.3 $\mu$m laser absorption sensor," Appl. Phys. B **110**, 359–365 (2013).
[20]Y. Deguchi, M. Noda, M. Abe, and M. Abe, "Improvement of combustion control through real-time measurement of O2 and CO concentrations in incinerators using diode laser absorption spectroscopy," Proc. Combust. Inst. **29**, 147–153 (2002).
[21]M. G. Allen, "Diode laser absorption sensors for gas-dynamic and combustion flows," Meas. Sci. Technol. **9**, 545–562 (1998).
[22]L. S. Rothman, I. E. Gordon, A. Barbe, D. C. Benner, P. F. Bernath, M. Birk *et al.*, "The HITRAN 2008 molecular spectroscopic database," J. Quant. Spectrosc. Radiat. Transfer **110**, 533–572 (2009).
[23]S. M. Abrarov, B. M. Quine, and R. K. Jagpal, "A simple interpolating algorithm for the rapid and accurate calculation of the Voigt function," J. Quant. Spectrosc. Radiat. Transfer **110**, 376–383 (2009).
[24]K. Madsen, H. B. Nielsen, and O. Tingleff, "Methods for non-linear least squares problems," IMM, DTU, 2004.
[25]S. Prucker, W. Meier, and W. Stricker, "A flat flame burner as calibration source for combustion research: Temperatures and species concentrations of premixed $H_2$/air flames," Rev. Sci. Instrum. **65**, 2908–2911 (1994).
[26]G. Sutton, A. Levick, G. Edwards, and D. Greenhalgh, "A combustion temperature and species standard for the calibration of laser diagnostic techniques," Combust. Flame **147**, 39–48 (2006).
[27]X. Liu, J. B. Jeffries, and R. K. Hanson, "Measurement of nonuniform temperature distributions using line-of-sight absorption spectroscopy," AIAA J. **45**, 411–419 (2007).
[28]W. Cai and C. F. Kaminski, "A tomographic technique for the simultaneous imaging of temperature, chemical species, and pressure in reactive flows using absorption spectroscopy with frequency-agile lasers," Appl. Phys. Lett. **104**, 034101 (2014).
[29]L. Ma and W. Cai, "Tomographic imaging of temperature and chemical species based on hyperspectral absorption spectroscopy," Opt. Express **17**, 8602–8613 (2009).